Electronic Supplementary Information

Experimental section

Materials: Sodium fluoride (NaF), acetone (C_3H_6O), anhydrous ethanol (C_2H_6O), ammonium chloride (NH_4Cl), sodium hydroxide (NaOH), salicylic acid ($C_7H_6O_3$), sodium citrate dihydrate ($C_6H_5Na_3O_7•2H_2O$), p–dimethylaminobenzaldehyde ($C_9H_{11}NO$), and sodium nitroferricyanide dihydrate ($C_5FeN_6Na_2O•2H_2O$) were purchased from Chengdu Kelong Ltd. High Purity Tungsten Sheet (W) was purchased from Runde Metal Materials Co., Ltd.

Preparation of WO_2/W: The polished W sheet was ultrasonically cleaned with acetone, ethanol, and deionized water for 10 min and dried in air. Then the W sheet was placed in an anodized electrolyte consisting of 0.5% NaF and 1 mol/L H_2SO_4 with the W sheet as the positive electrode and Pt plates as the negative electrode. The experiment was conducted for 60 minutes at a constant voltage of 40 V. The obtained WO_3 precursor was washed with ethanol and deionized water and dried and then sintered at 750 °C for 3 h in an argon−hydrogen atmosphere. Finally, WO_2 Nanoparticles on the W sheet can be obtained after cooling to room temperature.

Characterizations: The crystal structure of the prepared material was determined using an X-ray diffractometer with Cu Kα radiation (DX-2700B). microstructural observations were performed on a field−emission scanning electron microscopy (FEI Insect F50) and an atomic resolution scanning transmission electron microscopy (FEI Talos F200S Super). XPS measurements were carried out with Thermo Fischer ESCALAB Xi^+. The absorbance data were measured via an Ultraviolet-visible (UV–Vis) spectrophotometer (Shimazu UV–2600). EPR spectrum was recorded on a Brüker EMX spectrometer at room temperature.

Electrochemical measurements: All electrochemical measurements were carried out in an H−shaped electrochemical cell separated by Nafion 117 membrane using CHI 760E electrochemical workstation (Chenhua, Shanghai). The area of the working electrode immersed in the electrolyte is 0.25 cm^2. LSV was performed in Ar−saturated 0.1 M NaOH with 0.1 M $NaNO_2$ at a scan rate of 5 mV s^{-1}. All potentials reported in this work were converted to a reversible hydrogen electrode (RHE) scale, and current densities were normalized to the geometric surface area. All experiments were carried out at room temperature (25 °C).

Determination of NH_3: The NH_3 concentration in the electrolyte was determined (the obtained electrolyte was diluted 50 times) by the indophenol blue method. Specifically, 2 mL of electrolyte collected after electrolysis was mixed with 2 mL of coloring solution (1 M NaOH containing 5% salicylic acid and 5% sodium citrate), and 1 mL of oxidizing solution (0.05 M NaClO). Then 0.2 mL oxidation solution (0.05 M NaClO) mL catalyst solution (1 wt% $C_5FeN_6Na_2O$ $2H_2O$) was dropped into the collected solution. After standing in the dark for 2 h, the concentration of NH_3 was determined by UV-Vis at a specific wavelength of 655 nm. The concentration−absorbance curve was calibrated using the standard NH_4Cl solution with known concentrations of 0.0, 0.25, 0.5, 1.0, 2.0, and 5.0 μg mL^{-1} in 0.1 M NaOH. The fitting curve ($y = 0.43893x + 0.02172$, $R^2 = 0.9999$) shows good linear relation of absorbance value with NH_3 concentration.

Determination of NH_3 yield and FE:

The NH_3 FE is estimated from the charge consumed for NO_2^- reduction and the total charge passed through the electrode:

$$FE = 6 \times F \times V \times [NH_3] / (Q \times 17) \times 100\%$$

The yield rate of NH_3 (aq) is calculated:

$$NH_3 \text{ yield} = V \times [NH_3] / (A \times t \times 17)$$

Where $[NH_3]$ is the concentration of NH_3 (aq), F is the Faradaic constant (96485 C mol^{-1}), V is the volume of electrolyte in the anode compartment (45 mL), Q is the total charge passing the electrode, t is the electrolysis time, and A is the geometric surface area.

DFT calculation details: First−principles calculations with spin−polarized were performed based on density functional theory (DFT) implemented in the VASP package.[1] The projector augmented wave (PAW) method and generalized gradient approximation (GGA) of Perdew–Burke–Ernzerhof (PBE) was utilized to describe the interaction and electron exchange−correlation, respectively.[2,3] WO_2 slab structure was modeled, and the vacuum region's thickness is >15 Å to avoid spurious interaction. The cutoff energy was set to 450 eV. The Brillouin zone was sampled by 4 × 5 × 1 special k−points using the Monkhorst Pack scheme for structural configuration optimizations.[4] The force convergence thresholds are 0.02 eV/Å and the total energy is less than 1E−5 eV, respectively. The theoretical calculation results were processed and analyzed by VASPKIT software.[5]

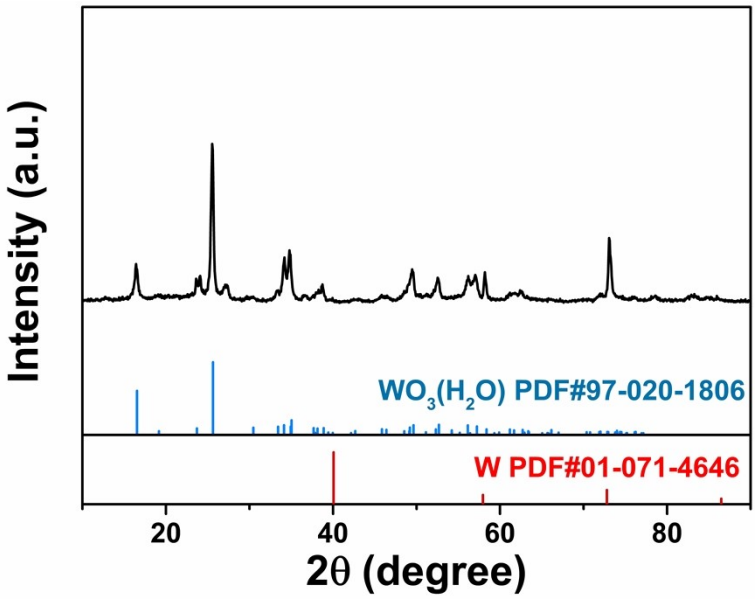

Fig. S1. XRD pattern of the anodized W plate.

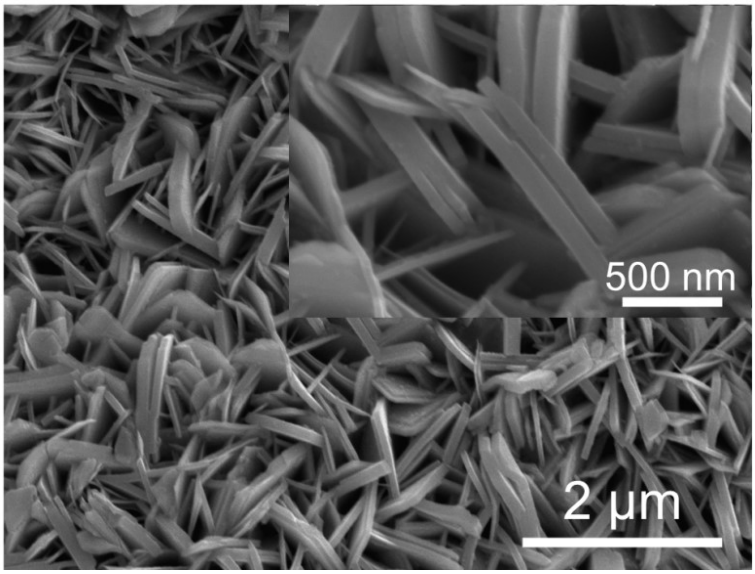

Fig. S2. SEM images of the anodized W plate.

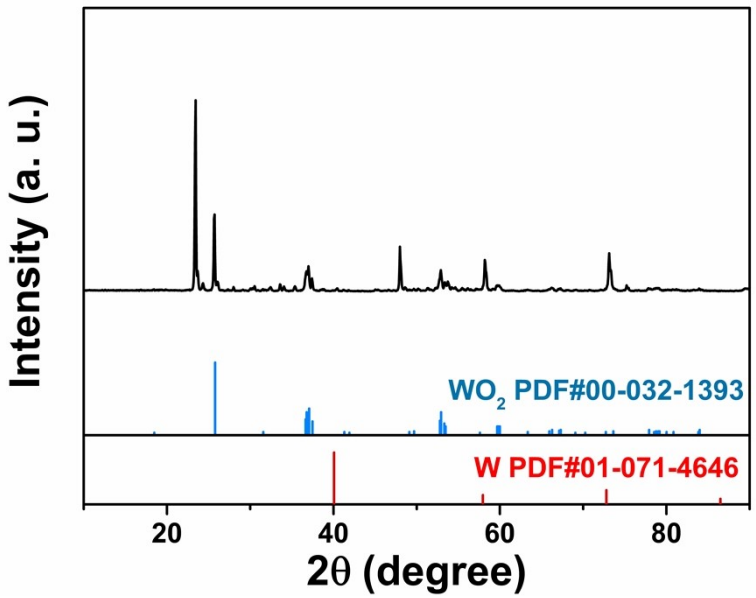

Fig. S3. XRD pattern of WO_2/W annealed at 700 °C.

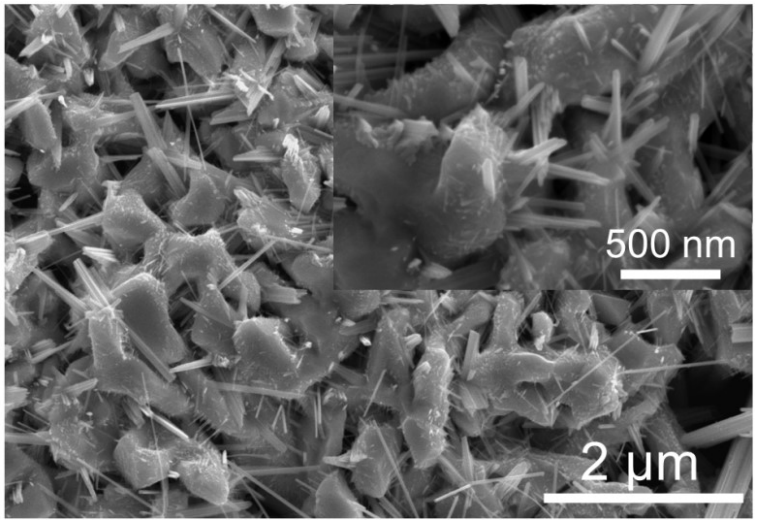

Fig. S4. SEM images of WO_2/W annealed at 700 °C.

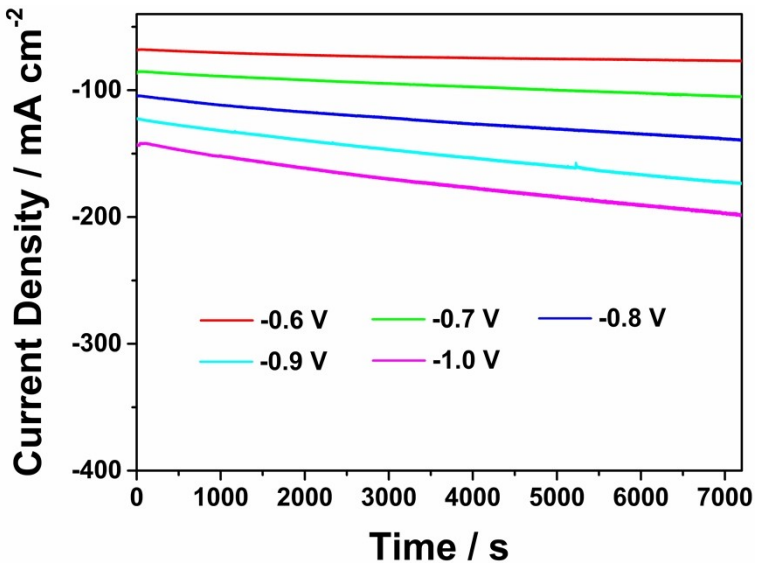

Fig. S5. Chronoamperometry curves of WO_2/W at each given potential.

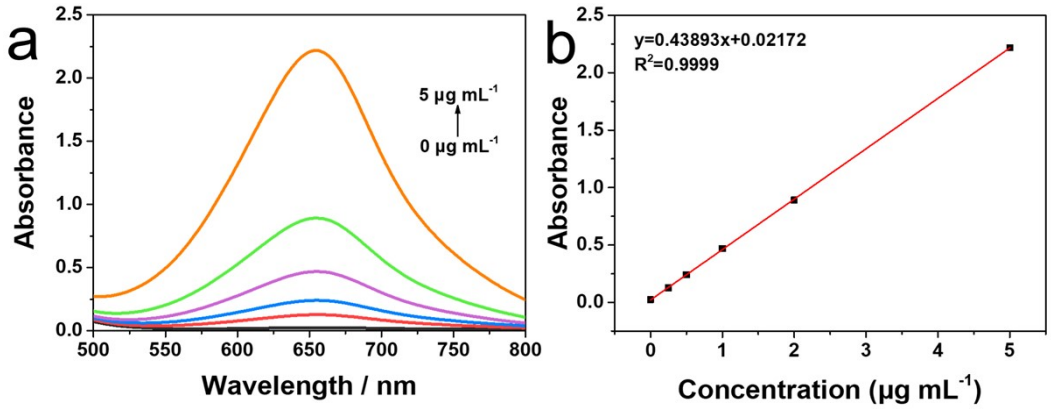

Fig. S6. (a) UV−Vis spectra and (b) corresponding calibration curves were used to calculate NH_4^+.

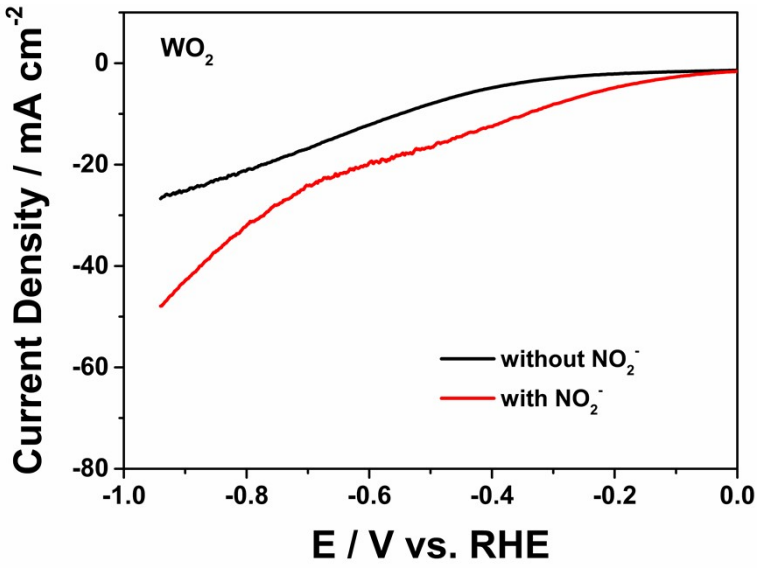

Fig. S7. LSV curves of WO_2/W in 0.1 M PBS with and without 0.1 M NO_2^-.

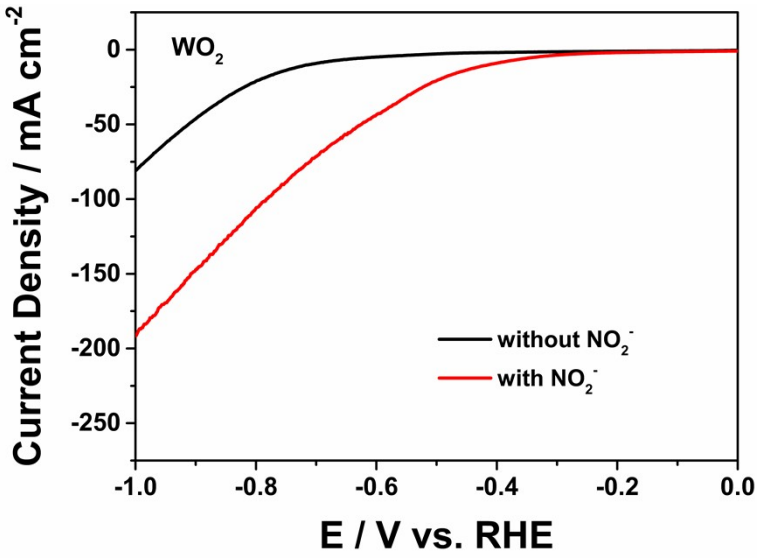

Figure S8. LSV curves of WO_2/W in 0.5 M Na_2SO_4 with and without 0.1 M NO_2^-.

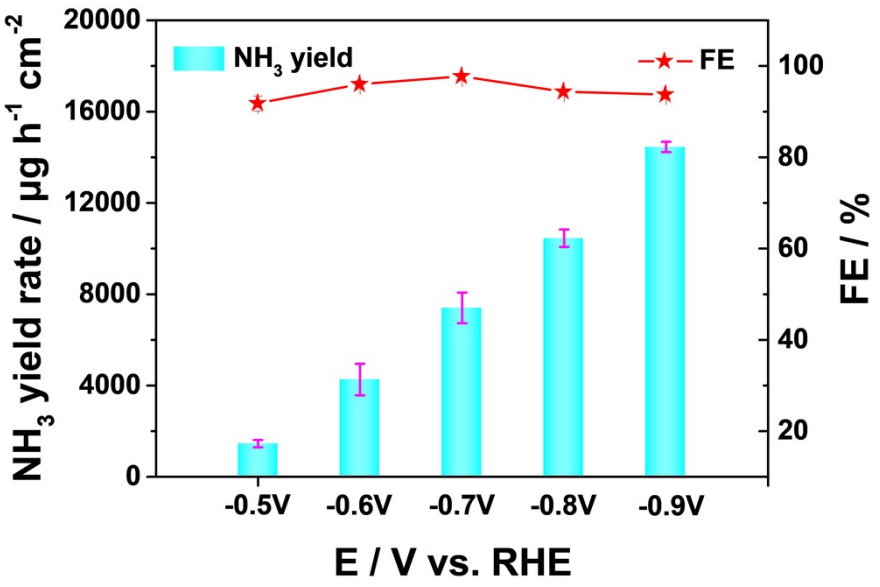

Figure S9. NH_3 yields and FEs of WO_2/W in 0.5 M Na_2SO_4 with 0.1 M NO_2^-.

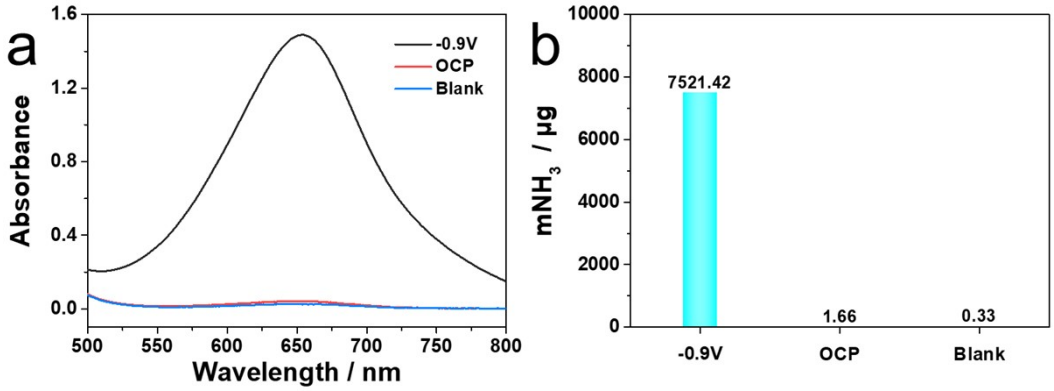

Fig. S10. (a) UV−Vis spectra and (b) amounts of electrogenerated NH_3 under different operating conditions.

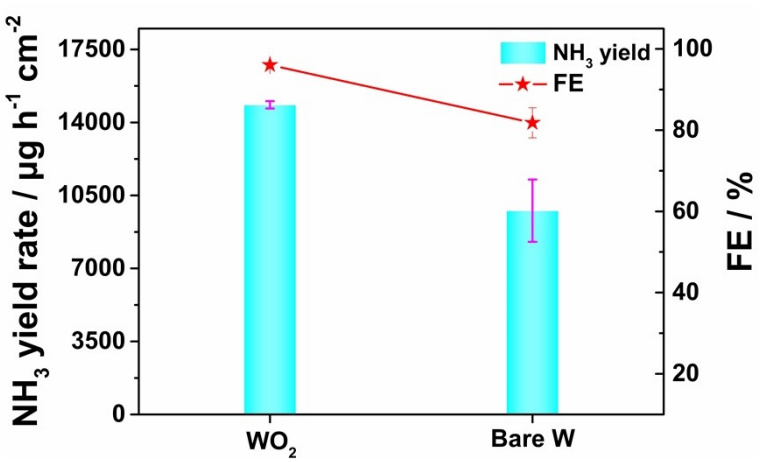

Fig. S11. NH_3 yields and FEs of WO_2/W and Bare W at −0.9 V.

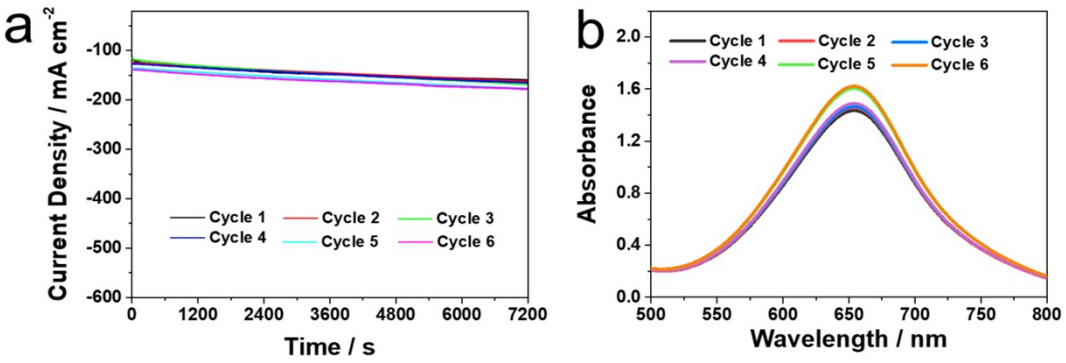

Fig. S12. (a) Chronoamperometry curves and (b) corresponding UV−Vis absorption spectra of WO_2/W for electrochemical catalytic production of NH_3 during cycling tests in 0.1 M NaOH with 0.1 M NO_2^- at −0.9 V.

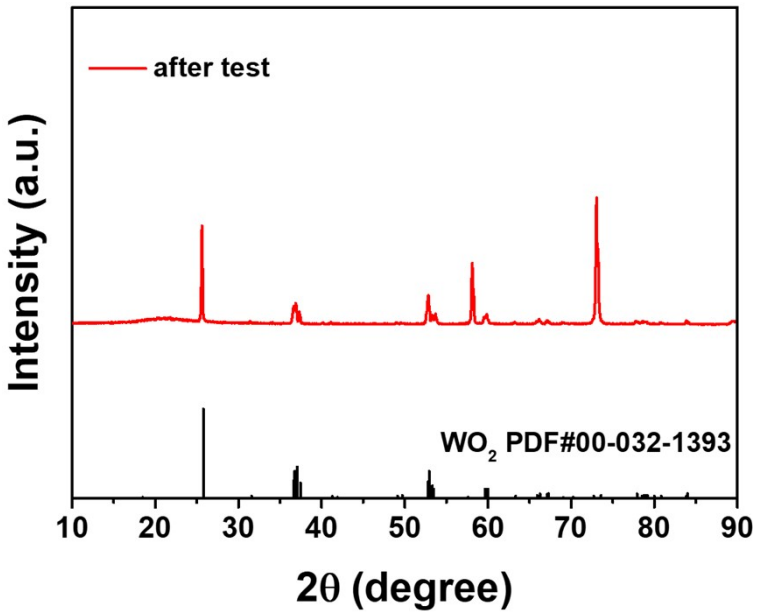

Fig. S13. XRD pattern of WO_2/W after long-term electrolysis.

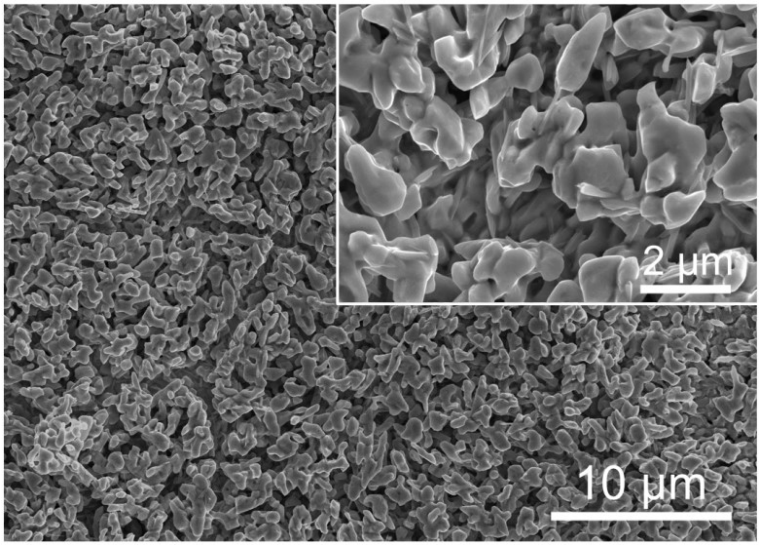

Fig. S14. SEM images of WO_2/W after long-term electrolysis.

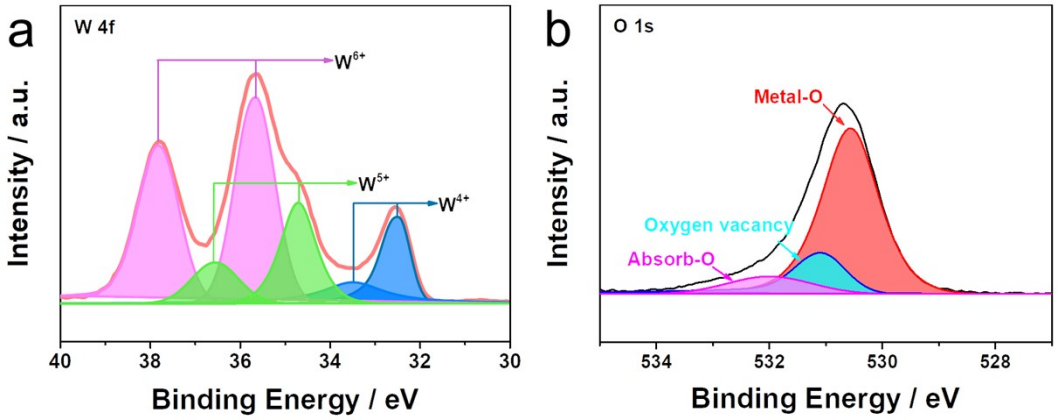

Fig. S15. (a) W 4f and (d) O 1s high-resolution spectra of WO_2/W after long-term electrolysis.

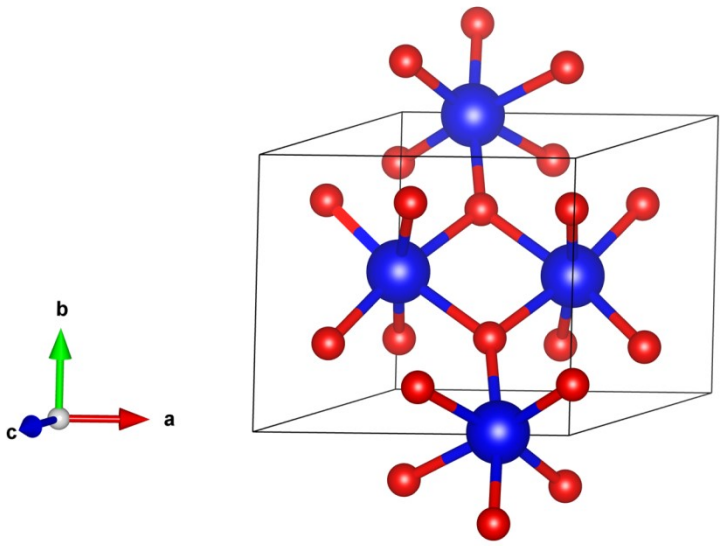

Fig. S16. Atomic configurations of WO_2 bulk.

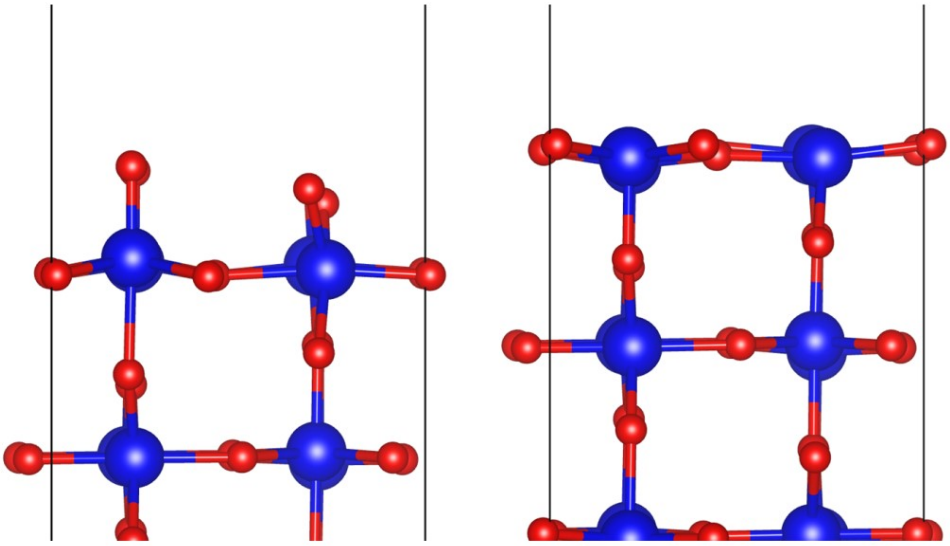

Fig. S17. Atomic configurations of WO_2 bulk. WO_2 (011) Slab models with two terminate surfaces, O end and WO end.

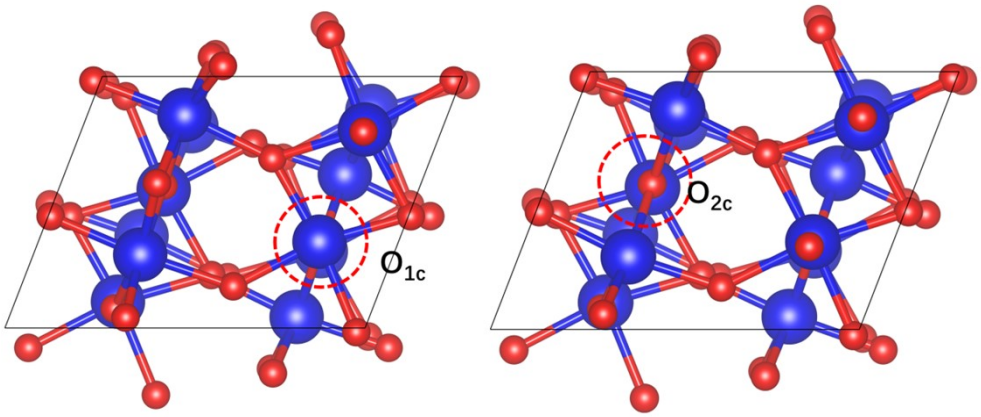

Fig. S18. WO_2 (011) Slab models with two types of OVs.

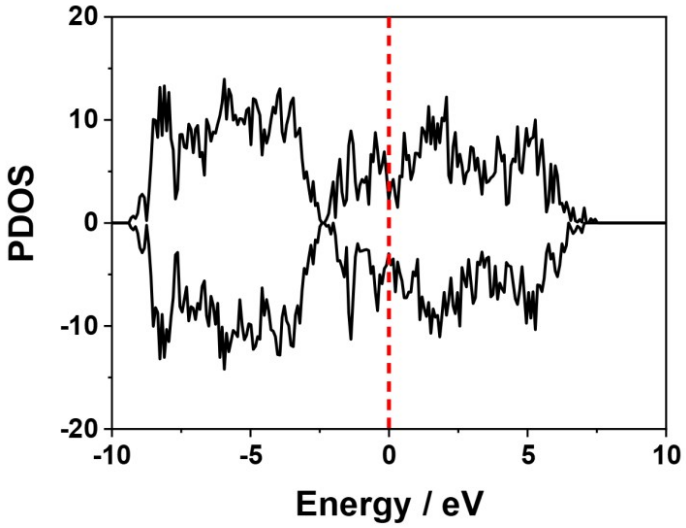

Fig. S19. PDOS of WO_2 (011) with O end terminate surface. Fermi levels are set at 0 eV.

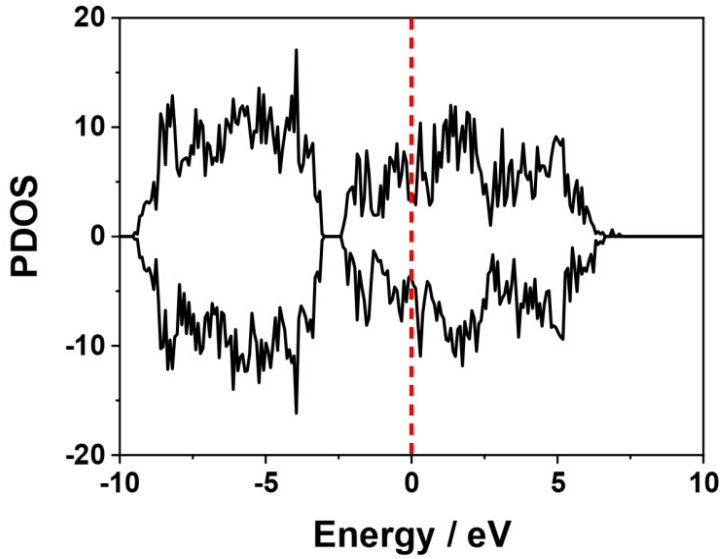

Fig. S20 PDOS of WO_2(011)−OV. Fermi levels are set at 0 eV.

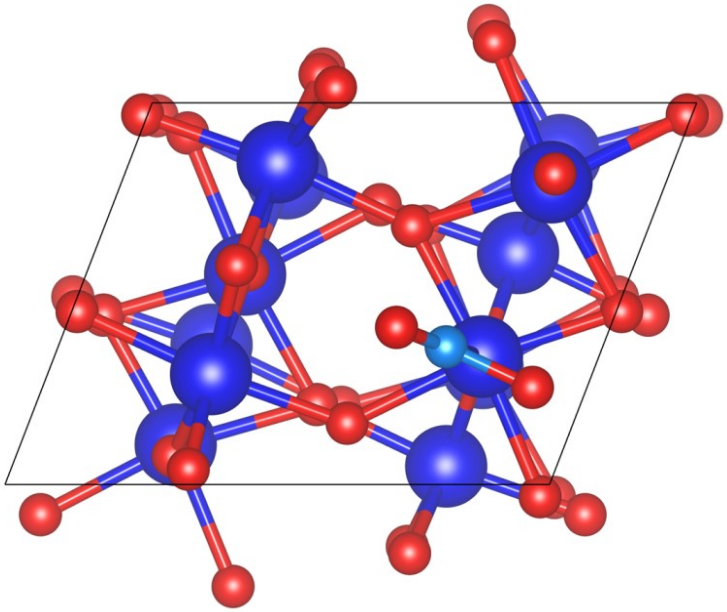

Fig. S21 The most stable NO_2 adsorption configuration on WO_2(011)−OV.

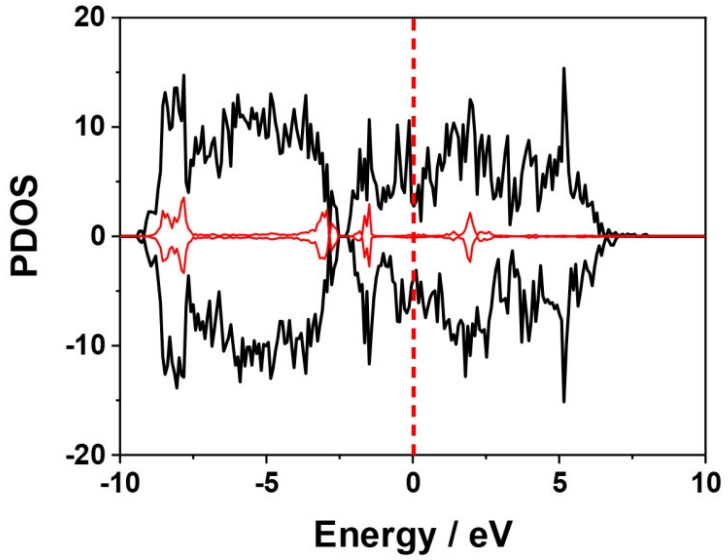

Fig. S22 PDOS of NO_2 adsorption on WO_2(011)−OV. Fermi levels are set at 0 eV.

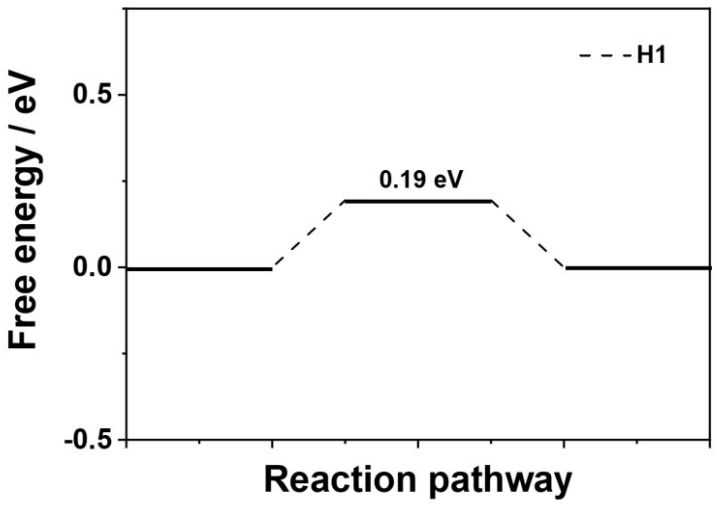

Fig. S23 Free energy diagram of HER processing on WO_2(011)−OV.

Table S1. Comparison of catalytic performance of WO_2/W with other reported NO_2^-RR electrocatalysts.

Catalyst	Electrolyte	FE (%)	NH_3 yield rate	Refs.
WO_2/W	**0.1 M NaOH (0.1 M $NaNO_2$)**	**94.32**	**14964.25 μg h^{-1} cm^{-2} (880.25 μmol cm^{-2})**	**This work**
CF@Cu_2O	0.1 M PBS (0.1 M $NaNO_2$)	94.2	441.8 μmol cm^{-2} h^{-1}	6
$[Co(DIM)Br_2]^+$	0.1 M $NaNO_2$	88	—	7
Oxo-MoS_x	0.1 M nitrite in 0.2 M citric acid (pH = 5)	13.5	—	8
$Cu_{80}Ni_{20}$	20 mM $NaNO_2$ (1.0 M NaOH)	87.6	—	9
Cu phthalocyanine	$NaNO_2$ (0.1 M KOH)	78	—	10
MnO_2 nanoarrays	0.1M Na_2SO_4 (4 mM $NaNO_2$)	6.0	3.09 × 10–11 mol s^{-1} cm^{-2}	11
Rh/Al_2O_3	25 mM phosphate Buffer+50 mM NO_2^-	68~95	—	12
Ni−NSA−V_{Ni}	0.2 M Na_2SO_4 (200 ppm NO_2^-)	88.9	235.98 μmol h^{-1} cm^{-2}	13
Cobalt-tripeptide complex	1.0 M MOPS buffer (1.0 M $NaNO_2$)	90±3	3.01 × 10^{-10} mol s^{-1} cm^{-2}	14
Poly-NiTRP complex	$NaNO_2$ (0.1 M $NaClO_4$)	—	1.1 mM	15
FeN_5H_2	1.0 M MOPS (1.0 M $NaNO_2$)	> 90	—	16
Cu_3P NA/CF	0.1 M PBS (0.1 M $NaNO_2$)	91.2 ± 2.5	1626.6 μg h^{-1} cm^{-2}	17

Table S2. Comparison of NH_3 yield and power density of our battery with recent Zn-N_2, Zn-NO, Zn-NO_2^-, or Zn-NO_3^- battery systems.

Catalyst	Battery Type	Power density (mW cm^{-2})	Refs.
WO_2/W	**Zn-NO_2^-**	**5.05**	**This work**
Cu NDs	Zn-N_2	0.0101	18
FeHTNs	Zn-N_2	0.01642	19
VN@NSC	Zn-N_2	0.01642	20
CoPi/HSNPC	Zn-N_2	0.31	21
NbS_2	Zn-N_2	0.31	22
CoPi/NPCS	Zn-N_2	0.49	23
Ti_2O_3	Zn-N_2	1.02	24
$FePS_3$	Zn-N_2	2.6	25
CoP	Zn-NO	0.496	26
NiO	Zn-NO	0.88	27
MoS_2	Zn-NO	1.04	28
Fe_2O_3	Zn-NO	1.18	29
Ni_2P	Zn-NO	1.53	30
TiO_2@Ti	Zn-NO	1.7	31
MoC	Zn-NO	1.8	32
VN	Zn-NO	2.0	33
CoS	Zn-NO	2.06	34
BiNDs	Zn-NO	2.33	35
Bi@C	Zn-NO	2.35	36
ITO@TiO_2TP	Zn-NO_2^-	1.22	37
A-TiO_{2-x}	Zn-NO_2^-	2.38	38
Co_3O_4	Zn-NO_2^-	6.03	39
TiO_2	Zn-NO_3^-	0.87	40
Fe/Ni_2P	Zn-NO_3^-	3.25	41
Co_2AlO_4	Zn-NO_3^-	3.43	42
CeO_2	Zn-NO_3^-	3.44	43
$NiCo_2O_4$	Zn-NO_3^-	3.94	44

References

1 G. Kresse and J. Hafner, *Phys. Rev. B*, 1994, **49**, 14251-14269.

2 G. Kresse and D. Joubert, *Phys. Rev. B*, 1999, **59**, 1758-1775.

3 J. P. Perdew, K. Burke and M. Ernzerhof, *Phys. Rev. Lett.*, 1996, **77**, 3865-3868.

4 H. J. Monkhorst and J. D. Pack, *Phys. Rev. B*, 1976, **13**, 5188-5192.

5 V. Wang, N. Xu, J.-C. Liu, G. Tang and W.-T. Geng, *Comput. Phys. Commun.*, 2021, **267**, 108033.

6 Q. Chen, X. An, Q. Liu, X. Wu, L. Xie, J. Zhang, W. Yao, M. S. Hamdy, Q. Kong and X. Sun, *Chem. Commun.*, 2022, **58**, 517-520.

7 S. Xu, H.-Y. Kwon, D. C. Ashley, C.-H. Chen, E. Jakubikova and J. M. Smith, *Inorg. Chem.*, 2019, **58**, 9443-9451.

8 D. He, Y. Li, H. Ooka, Y. K. Go, F. Jin, S. H. Kim and R. Nakamura, *J. Am. Chem. Soc.*, 2018, **140**, 2012-2015.

9 L. Mattarozzi, S. Cattarin, N. Comisso, P. Guerriero, M. Musiani, L. Vázquez-Gómez and E. Verlato, *Electrochim. Acta*, 2013, **89**, 488-496.

10 N. Chebotareva and T. Nyokong, *J. Appl. Electrochem.*, 1997, **27**, 975-981.

11 R. Wang, Z. Wang, X. Xiang, R. Zhang, X. Shi and X. Sun, *Chem. Commun.*, 2018, **54**, 10340-10342.

12 C. A. Clark, C. P. Reddy, H. Xu, K. N. Heck, G. Luo, T. P. Senftle and M. S. Wong, *ACS Catal.*, 2019, **10**, 494-509.

13 C. Wang, W. Zhou, Z. Sun, Y. Wang, B. Zhang and Y. Yu, *J. Mater. Chem. A*, 2021, **9**, 239-243.

14 Y. Guo, J. R. Stroka, B. Kandemir, C. E. Dickerson and K. L. Bren, *J. Am. Chem. Soc.*, 2018, **140**, 16888-16892.

15 P. Dreyse, M. Isaacs, K. Calfumán, C. Cáceres, A. Aliaga, M. J. Aguirre and D. Villagra, *Electrochim. Acta*, 2011, **56**, 5230-5237.

16 J. R. Stroka, B. Kandemir, E. M. Matson and K. L. Bren, *ACS Catal.*, 2020, **10**, 13968-13972.

17 J. Liang, B. Deng, Q. Liu, G. Wen, Q. Liu, T. Li, Y. Luo, A. A. Alshehri, K. A. Alzahrani and D. Ma, *Green Chem.*, 2021, **23**, 5487-5493.

18 C. Du, Y. Gao, J. Wang and W. *Chem. Commun.*, 2019, **55**, 12801-12804.

19 X.-W. Lv, X.-L. Liu, L.-J. Gao, Y.-P. Liu and Z.-Y. Yuan, *J. Mater. Chem. A*, 2021, **9**, 4026-4035.

20 X.-W. Lv, Y. Liu, Y.-S. Wang, X.-L. Liu and Z.-Y. Yuan, *Appl. Catal. B*, 2021, **280**, 119434.

21 J.-T. Ren, L. Chen, Y. Liu and Z.-Y. Yuan, *J. Mater. Chem. A*, 2021, **9**, 11370-11380.

22 H. Wang, J. Si, T. Zhang, Y. Li, B. Yang, Z. Li, J. Chen, Z. Wen, C. Yuan, L. Lei and Y. Hou, *Appl. Catal. B*, 2020, **270**, 118892.

23 J. T. Ren, L. Chen, H. Y. Wang and Z. Y. Yuan, *ACS Appl. Mater. Interfaces*, 2021, **13**, 12106-12117.

24 H.-j. Chen, Z.-q. Xu, S. Sun, Y. Luo, Q. Liu, M. S. Hamdy, Z.-s. Feng, X. Sun

and Y. Wang, *Inorg. Chem. Front.*, 2022, **9**, 4608-4613.

25 H. Wang, Z. Li, Y. Li, B. Yang, J. Chen, L. Lei, S. Wang and Y. Hou, *Nano Energy*, 2021, **81**.

26 J. Liang, W.-F. Hu, B. Song, T. Mou, L. Zhang, Y. Luo, Q. Liu, A. A. Alshehri, M. S. Hamdy, L.-M. Yang and X. Sun, *Inorg. Chem. Front.*, 2022, **9**, 1366-1372.

27 P. Liu, J. Liang, J. Wang, L. Zhang, J. Li, L. Yue, Y. Ren, T. Li, Y. Luo, N. Li, B. Tang, Q. Liu, A. M. Asiri, Q. Kong and X. Sun, *Chem. Commun.*, 2021, **57**, 13562-13565.

28 L. Zhang, J. Liang, Y. Wang, T. Mou, Y. Lin, L. Yue, T. Li, Q. Liu, Y. Luo, N. Li, B. Tang, Y. Liu, S. Gao, A. A. Alshehri, X. Guo, D. Ma and X. Sun, *Angew. Chem. Int. Ed*, 2021, **60**, 25263-25268.

29 J. Liang, H. Chen, T. Mou, L. Zhang, Y. Lin, L. Yue, Y. Luo, Q. Liu, N. Li, A. A. Alshehri, I. Shakir, P. O. Agboola, Y. Wang, B. Tang, D. Ma and X. Sun, *J. Mater. Chem. A*, 2022, **10**, 6454-6462.

30 T. Mou, J. Liang, Z. Ma, L. Zhang, Y. Lin, T. Li, Q. Liu, Y. Luo, Y. Liu, S. Gao, H. Zhao, A. M. Asiri, D. Ma and X. Sun, *J. Mater. Chem. A*, 2021, **9**, 24268-24275.

31 J. Liang, P. Liu, Q. Li, T. Li, L. Yue, Y. Luo, Q. Liu, N. Li, B. Tang, A. A. Alshehri, I. Shakir, P. O. Agboola, C. Sun and X. Sun, *Angew. Chem. Int. Ed*, 2022, **61**, e202202087.

32 G. Meng, M. Jin, T. Wei, Q. Liu, S. Zhang, X. Peng, J. Luo and X. Liu, *Nano*

Res., 2022, DOI: 10.1007/s12274-022-4747-y.

33 D. Qi, F. Lv, T. Wei, M. Jin, G. Meng, S. Zhang, Q. Liu, W. Liu, D. Ma, M. S. Hamdy, J. Luo and X. Liu, *Nano Res. Energy*, 2022, **1,** e9120022.

34 L. Zhang, Q. Zhou, J. Liang, L. Yue, T. Li, Y. Luo, Q. Liu, N. Li, B. Tang, F. Gong, X. Guo and X. Sun, *Inorg. Chem.*, 2022, **61**, 8096-8102.

35 Y. Lin, J. Liang, H. Li, L. Zhang, T. Mou, T. Li, L. Yue, Y. Ji, Q. Liu, Y. Luo, N. Li, B. Tang, Q. Wu, M. S. Hamdy, D. Ma and X. Sun, *Mater. Today Phys.*, 2022, **22**.

36 Q. Liu, Y. Lin, L. Yue, J. Liang, L. Zhang, T. Li, Y. Luo, M. Liu, J. You, A. A. Alshehri, Q. Kong and X. Sun, *Nano Res.*, 2022, **15**, 5032-5037.

37 S. Li, J. Liang, P. Wei, Q. Liu, L. Xie, Y. Luo and X. Sun, *eScience*, 2022, **2**, 382-388.

38 Z. Ren, Q. Chen, X. An, Q. Liu, L. Xie, J. Zhang, W. Yao, M. S. Hamdy, Q. Kong and X. Sun, *Inorg. Chem.*, 2022, **61**, 12895-12902.

39 R. Zhang, S. Zhang, Y. Guo, C. Li, J. Liu, Z. Huang, Y. Zhao, Y. Li and C. Zhi, *Energy & Environmental Science*, 2022, **15**, 3024-3032.

40 Y. Guo, R. Zhang, S. Zhang, Y. Zhao, Q. Yang, Z. Huang, B. Dong and C. Zhi, *Energy Environ. Sci.*, 2021, **14**, 3938-3944.

41 R. Zhang, Y. Guo, S. Zhang, D. Chen, Y. Zhao, Z. Huang, L. Ma, P. Li, Q. Yang, G. Liang and C. Zhi, *Adv. Energy Mater.*, 2022, **12**.

42 Z. Deng, J. Liang, Q. Liu, C. Ma, L. Xie, L. Yue, Y. Ren, T. Li, Y. Luo, N. Li, B. Tang, A. Ali Alshehri, I. Shakir, P. O. Agboola, S. Yan, B. Zheng, J. Du, Q.

Kong and X. Sun, *Chem. Eng. J.*, 2022, **435**.

43 Z. Li, Z. Deng, L. Ouyang, X. Fan, L. Zhang, S. Sun, Q. Liu, A. A. Alshehri, Y. Luo, Q. Kong and X. Sun, *Nano Res.*, 2022, DOI: 10.1007/s12274-022-4863-8.

44 Q. Liu, L. Xie, J. Liang, Y. Ren, Y. Wang, L. Zhang, L. Yue, T. Li, Y. Luo, N. Li, B. Tang, Y. Liu, S. Gao, A. A. Alshehri, I. Shakir, P. O. Agboola, Q. Kong, Q. Wang, D. Ma and X. Sun, *Small*, 2022, **18,** 2106961.